European Journal of Agronomy 127 (2021) 126287

Contents lists available at ScienceDirect

European Journal of Agronomy

journal homepage: www.elsevier.com/locate/eja

Simultaneous assessment of nitrogen and water status in winter wheat using hyperspectral and thermal sensors

J.L. Pancorbo [a], C. Camino [b], M. Alonso-Ayuso [a], M.D. Raya-Sereno [a], I. Gonzalez-Fernandez [c], J. L. Gabriel [a,d], P.J. Zarco-Tejada [e,f], M. Quemada [a,*]

[a] *Universidad Politécnica de Madrid, CEIGRAM, Madrid, Spain*
[b] *European Commission (EC), Joint Research Centre (JRC), Ispra, Italy*
[c] *Ecotoxicology of Air Pollution, CIEMAT, Madrid, Spain*
[d] *Instituto Nacional de Investigación y Tecnología Agraria y Alimentaria (INIA-INAGEA), Madrid, Spain*
[e] *School of Agriculture and Food, Faculty of Veterinary and Agricultural Sciences (FVAS) & Melbourne School of Engineering (MSE), University of Melbourne, Melbourne, VIC, Australia*
[f] *Instituto de Agricultura Sostenible (IAS), Consejo Superior de Investigaciones Científicas (CSIC), Alameda del Obispo s/n, 14004, Córdoba, Spain*

A R T I C L E I N F O

Keywords:
Confounding effects
Critical nitrogen dilution curve
Crop sensors
Fertilization
Irrigation
Remote sensors
Soil background

A B S T R A C T

Remote sensing is a valuable tool for reducing the environmental impact of agricultural practices by detecting crop nitrogen (N) and water status for site-specific N fertilization and irrigation. The interaction between N and water status may produce confounding effects in the acquired spectral reflectance, making it difficult to separate crop deficiencies. The objective of this study was to evaluate the potential of visible and infrared hyperspectral and thermal imaging sensors for N and water status assessment with reduced confounding effects. A winter wheat (*Triticum aestivum* L.) field experiment combining four N and two irrigation levels was conducted in Central Spain over 2 years. The Nitrogen Nutrition Index (NNI) was monitored (mid stem elongation, final stem elongation, flowering stage) and the crop water status was measured with a leaf porometer at flowering. Two hyperspectral sensors covering the visible and near infrared regions (400–850 nm) and part of the short-wave infrared (950–1750 nm) together with a thermal camera were installed on-board an aircraft to acquire images 300 m above the experiment. In addition, canopy reflectance (400−1000 nm) was measured with a handheld spectroradiometer at ground level. The relationship between the ground-based determination of N and water status with indicators based on remote sensors was analyzed. The planar domain Canopy Chlorophyll Content Index (CCCI) reduced soil background noise and correlated with the NNI in all cases ($R^2 > 0.44$; $P < 0.001$). Reliable assessment of water status was achieved by using the Water Deficit Index (WDI), which is calculated using the Vegetation Index-Temperature trapezoid. The CCCI distinguished between N levels reducing the confounding effect of the water status, in contrast to the WDI which was mostly affected by the water status. Combining the CCCI and WDI to assess the crop NNI reduced the root mean square error to 0.109, suggesting that the combination of spectral and thermal information could improve the adjustment of N fertilization and irrigation to crop requirements. However, the approach must be validated in other cultivars and environments before making N fertilization and irrigation recommendations.

1. Introduction

According to the FAO, in 2018, 15 % of the total area harvested in the world by primary crops was wheat, which received 17 % of total world nitrogen (N) fertilizer consumption (FAOstat, 2020). Adjusting fertilization and irrigation to winter wheat requirements is a crucial strategy for increasing N use efficiency (NUE) and water use efficiency (WUE) while reducing water and soil pollution (Arregui et al., 2006) and greenhouse gas emissions (Aguilera et al., 2013). In recent years many attempts have been made to develop accurate techniques to determine crop status and adjust fertilization and irrigation to crop demand. However, each crop requires a specific strategy for adjusting N fertilizer application because crop N demand changes with time, biomass accumulation and crop development (Sticksel et al., 1999). Along these lines,

* Corresponding author.
E-mail address: miguel.quemada@upm.es (M. Quemada).

https://doi.org/10.1016/j.eja.2021.126287
Received 31 August 2020; Received in revised form 6 April 2021; Accepted 8 April 2021
Available online 18 April 2021
1161-0301/© 2021 Elsevier B.V. All rights reserved.

monitoring temporal variations of crop N status could allow adapting N application to crop N requirements (Quemada et al., 2014). In winter wheat, a common strategy is to split fertilization into two topdressing N fertilizer applications: one at the beginning of tillering and the rest during stem elongation to ensure yield (Arregui et al., 2006). Consequently, it is crucial to determine crop status at early stages to adjust fertilizer rates (Raun et al., 2005; Ravier et al., 2017). Additionally, N and water availability between the late boot stage and early grain filling determine grain quality (Ottman et al., 2000) and so crop status information is crucial for guiding crop management during these growth stages (Zhao et al., 2005; Diacono et al., 2013).

The Nitrogen Nutrition Index (NNI) is a well-known indicator of crop N status (Justes et al., 1994). NNI compares N concentration in leaves and shoots (%N) with the critical %N at a given biomass. Critical %N is the minimum %N that produces the maximum growth rate of biomass. Critical %N decreases with biomass production, given the N critical dilution curve (CDC) that is enveloped by minimum and maximum limits (Greenwood et al., 1990). For a given biomass, if the actual NNI value is below the minimum threshold, N is limiting crop growth. Water deficit has a direct effect on plant N demand because it reduces growth and affects the partitioning between structural and metabolic tissues (Sadras and Lemaire, 2014). For this reason, efforts have been made to develop an alternative CDC for winter wheat under water deficit regimes (Hoogmoed and Sadras, 2018; Neuhaus et al., 2017) or for spring wheat, often exposed to limited water availability (Ziadi et al., 2010).

Based on the CDC approach, N demand can be monitored by continuous determination of %N in a representative sample of known aerial biomass (Mistele and Schmidhalter, 2008). However, this procedure is expensive, slow and hard to apply to large fields (Haboudane et al., 2002; Min and Lee, 2005). In addition, by the time the results are available, in many cases the phenological stage of the crop has changed and it is of little support for making decisions related to fertilization. These limitations could be overcome by remote sensing techniques (Raya-Sereno et al., 2021). Even though its widespread use is relatively new (Weiss et al., 2020), this approach provides valuable insights into improving the estimation of N status in large areas (Hatfield et al., 2008). The remote sensing techniques are based on a sensor that measures surface temperature or canopy reflectance at different wavelengths of the electromagnetic spectrum, requiring corrections because of atmospheric disturbances (Griffin and Burke, 2003). Canopy reflectance is affected by vegetation structure, crop photosynthetic pigments related to the N concentration (Gabriel et al., 2017) and other factors affecting crop development, such as water content (Chen et al., 2005).

Moreover, a number of limitations arise when using spectral information for estimating crop biophysical parameters: when canopy reflectance is measured with different sensors, discrepancies can be found due to differences in spectral resolution, view angle or atmospheric corrections, among others (Cross et al., 2018). At early growth stages (GS), before achieving full canopy cover, soil background affects the reflectance, making it difficult to distinguish between soil and plant spectral components. This is a critical issue because decisions based on N fertilization rates are made at early stages (Basso et al., 2009). Thus, reliable N estimations at early GS have been the focus of research, such as the development of the Canopy Chlorophyll Content Index (CCCI) (Barnes et al., 2000), which is a planar domain Vegetation Index (VI) that measures plant biophysical parameters in a mixed soil/plant pixel by analyzing the relationship between one chlorophyll and one biomass related VI plotted in a two dimensional space (Clarke et al., 2001). Another limitation when determining crop N status is that most VIs have been developed to estimate chlorophyll content or biomass without considering the N dilution effects (Mistele and Schmidhalter, 2008). Nevertheless, optimal %N is dependent on the biomass, and it changes with crop development (Lemaire et al., 2008; Sadras and Lemaire, 2014). Also, water and N shortage affect the reflected light acquired by the sensor, and it can be difficult to identify the stress suffered by the crop (Barnes et al., 2000; Osborne et al., 2002; Tilling et al., 2007; Cossani and Sadras, 2018). In addition, the ability of estimating crop parameters through VIs is reduced when the crop is experiencing water stress (Schepers et al., 1996; Kusnierek and Korsaeth, 2015).

Stomatal conductance depends on different environmental factors including soil water availability and is directly related to plant photosynthesis and transpiration (Constable and Rawson, 1980). A reliable assessment of this variable can be achieved with a leaf porometer (Möller et al., 2007; Masseroni et al., 2017). The transpiration rate is inversely correlated with leaf temperature; for this reason, foliar temperature has long been used to detect plant water stress (Tanner, 1963) and the correlation of temperature-based indicators with stomatal conductance is well documented (Jones, 1999; Grant et al., 2007). The foliage and air temperature difference has proven to be a reliable method to detect plant water stress (Idso et al., 1977). However, this alone is not enough to detect plant water stress because other environmental factors different from water supply influence plant temperature (Walker, 1980; Heitholt et al., 1991). To overcome this limitation, Idso et al. (1981) developed the Crop Water Stress Index (CWSI) by normalizing the foliage-air temperature difference with the vapour pressure deficit (VPD), allowing comparison between vegetation at different environmental conditions and dates. The CWSI is based on the ratio between actual and potential transpiration, calculated as the relationship between the distance to minimum and maximum water stress baselines. Some problems are present when applying the CWSI with airborne thermal sensors under partially vegetated fields: the information is taken from soil-plant mixed pixels, and soil and plant thermal emission can be drastically different (Jackson et al., 1981; Rodriguez et al., 2005). To solve this problem, Moran et al. (1994) proposed the Water Deficit Index (WDI), which is calculated by plotting in a two dimensional space the canopy-air temperature difference and the ground cover simulated by a spectral VI using the concept of the Vegetation index-Temperature (VIT) trapezoid.

The aim of this study was to evaluate the potential of different spectral- and temperature-based indicators for simultaneous crop N and water status assessment by reducing the potential confounding effects in winter wheat. In order to reinforce the results, the reflectance was measured at ground level and with an airborne platform 300 m above the experiment using two hyperspectral sensors. The specific objectives were i) to identify the best hyperspectral VI and temperature-based indicator for the NNI and water status assessment ii) to combine the best NNI and water status predictors to develop an improved indicator for N status monitoring, and iii) to evaluate the capacity of the indicators to identify N and water levels with minimum confounding effects.

2. Materials and methods

2.1. Experimental design

The study was carried out at La Chimenea farm station (40°04′N, 03°32′W, 550 m a.s.l.), near Aranjuez (Madrid, Spain) during two consecutive growing seasons: 2017/2018 and 2018/2019 (hereinafter referred to as 2018 and 2019, respectively). The study site was flat (slope $<$ 1%) and the soil, representative of the medium Tajo River terraces, is mapped as *Haplic Calcisol* (World Reference Base for Soil Resources, 2014), with a pH ≈ 8.1, medium organic matter content (topsoil organic C 1.01 g kg^{-1}), and a silty clay loam texture with low stone content throughout the soil profile. The climate of the area is classified as cold semi-arid (Bsk) according to the Köppen classification, with a mean annual temperature of 14.2 °C and 373 mm of average rainfall. Usually, spring and summer are characterized by a substantial water deficit that is compensated by irrigation, water-delivered since April. High inter-annual variability is characteristic of the region; therefore, relevant climate variables were recorded hourly throughout the experimental period with a weather station located at the farm.

The experiment was conducted in a field irrigated by a full circular pivot (220 m radius) for uniform and adjustable water delivery. At the beginning of each growing season (02/11/2017; 17/11/2018) a different quarter of the field was sown with winter wheat (*Triticum aestivum* L, cv. Nogal) at a seeding rate of 220 kg seeds ha^{-1} (5.6 × 10^6 seeds ha^{-1}). To ensure uniformity and low levels of soil inorganic N content, both quarters of the field had a maize crop (*Zea mays* L.) that did not receive mineral N fertilizer previous to the wheat and had not received organic amendments during the 4 years prior to the beginning of the trial. To establish a factorial experiment, 32 plots (25 × 25 m in 2018 and 22 × 22 m in 2019) were marked and randomly assigned into four N and two water levels, with four replications (Fig. 1). The plots were georeferenced by RTK (Real Time Kinematic) through the National Geodetic Network of Reference Stations GNSS (ERGNSS) technique, using the permanent Sonseca (Toledo) and Aranjuez (Madrid) stations due to their proximity, with a Topcon HiPer Pro receptor® (Topcon Singapore Holdings Pte. Ltd, Singapore).

The four N levels were established by applying N fertilizer (calcium ammonium nitrate) from 0 to above the recommended dose, in 50 kg N ha^{-1} increments. The wheat N requirements were calculated as the product of the expected grain yield (6.5 Mg ha^{-1}) times an extraction coefficient of 30 kg N Mg^{-1} (Arregui et al., 2006). Fertilizer rates applied to each N level were 0, 50, 100 and 150 kg N ha^{-1} for N0, N1, N2 and N3, respectively in 2018; and 0, 42, 92 and 142 kg N ha^{-1} in 2019. N fertilizer was hand-broadcasted to plots in two growth stages (Zadoks et al., 1974): two thirds at tillering (Z22; 25/01/2018 and 30/01/2019) and one third at stem elongation (Z35; 22/03/2018) or final stem elongation (Z39; 15/04/2019). Before the first fertilizer application each year, soil samples from 0−0.6 m in 0.2 m depth intervals were taken from each plot to determine soil mineral N content (kg N ha^{-1}). Soil sub-samples were extracted with 1 M KCl, and analyzed for N-NH_4^+ and N-NO_3- (Keeney and Nelson, 1982). Soil mineral N was calculated as the addition of N-NH_4^+ and N-NO_3- content in the top 0.60 m, and was 36 kg N ha^{-1} in 2018 and 57 kg N ha^{-1} in 2019. The N available in each treatment was calculated by adding the N applied with the fertilizer to the soil mineral N content before fertilizer application. Before sowing wheat, phosphorus (50 kg P ha^{-1}) and potassium (70 kg K ha^{-1}) were applied so that crop growth would not be limited.

To evaluate the effect of water availability on monitoring crop N status by optical and thermal sensors, half of the plots (Fig. 1) were irrigated at the beginning of flowering (Z63) in both experimental years. In 2018, half of the plots received 25 mm of water on May 8th. In 2019, half of the plots were irrigated in two events (30 mm on May 7th and 9 mm on May 10th). Additionally, due to the scarcity of winter rainfall in 2019 all plots were irrigated twice with 25 mm at Z32 (13/03/2019) and Z39 (15/04/2019) (Fig. 2). In the text, the plots that did not receive irrigation at flowering are referred to as W1, and the others as W2.

2.2. Crop analyses

Two samples (0.5 × 0.5 m) of aerial biomass per plot were collected three times each experimental year at mid stem elongation, final stem elongation, and flowering (Table 1). The samples were dried at 65 °C for 48 h and weighed to determine aerial biomass (kg ha^{-1}). A subsample was analyzed to calculate N concentration (%N) by using the Dumas combustion method (LECO FP-428 analyzer, St. Joseph, MI, USA). At flowering, spikes and the rest of aerial biomass were analyzed separately and %N was calculated using the relative weights of shoots + leaves and spikes.

The first sampling campaign was conducted between the first and second N fertilizer application, as it might be important for adjusting the second N application. The second sampling campaign was conducted just before flowering, when maximum ground cover and N uptake were reached. Crop N status measurements at this stage indicate if foliar N application would increase grain protein content (Angus and Fischer,

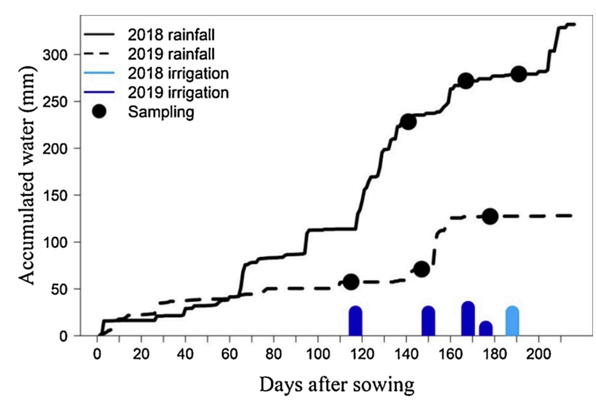

Fig. 2. Total amount of rainfall (mm) and irrigation over the two experimental years. Only half of the experiment was irrigated at flowering. Dots indicate the dates of on-ground sampling.

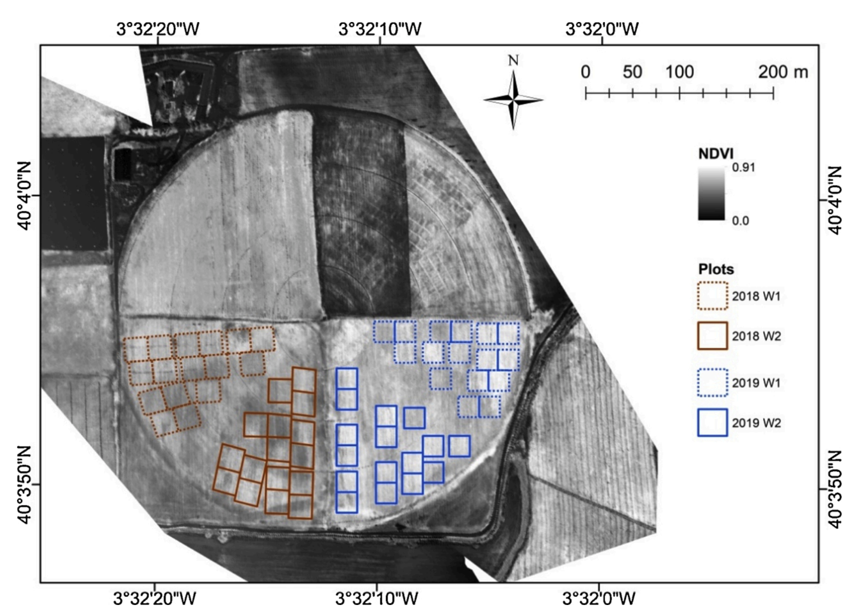

Fig. 1. Normalized Difference Vegetation Index (NDVI) retrieved from the airborne hyperspectral VNIR imager at final stem elongation in 2019. The 32 plots monitored each year separated by water levels (W1, W2) are shown.

Table 1
Growth stages, dates and Zadoks stages (Z) of biomass sampling and sensor measurement acquisition.

	Mid stem elongation		Final stem elongation		Flowering	
	Dates	Zadoks	Dates	Zadoks	Dates	Zadoks
Biomass	22/03/2018	Z34	17/04/2018	Z37	11/05/2018	Z65
	11/03/2019	Z32	12/04/2019	Z39	13/05/2019	Z65
FieldSpec	22/03/2018	Z34	17/04/2018	Z37	11/05/2018	Z65
	08/03/2019	Z32	12/04/2019	Z39	14/05/2019	Z65
Aircraft	–	–	19/04/2018	Z37	15/05/2018	Z65
	11/03/2019	Z32	12/04/2019	Z39	16/05/2019	Z65

1991). The third sampling campaign was carried out at full flowering, when N translocation to spikes had already started and the experiment was split into two water levels.

To determine crop N status, the NNI was calculated by using the CDC (Eq. 1) for winter wheat proposed by Justes et al. (1994):

$$\%N_c = a \text{ x Biomass }^{-b} \tag{1}$$

where $\%N_c$ is the minimum N concentration that produces the maximum growth at a given shoot *Biomass*, and $a = 5.35$ and $b = 0.442$ are estimated parameters. The parameter a represents the total shoots biomass for 1 Mg DM ha^{-1}, and b the coefficient of dilution. The actual ratio of % N and aerial biomass determined in the samples collected from the experimental plots was used to calculate the NNI following the equation:

$$NNI = \frac{\%N}{\%N_c} \tag{2}$$

Therefore, values of NNI close to 1 represent vegetation with N fertilization adjusted to crop requirement, while values above 1 represent overfertilized vegetation and below 1, vegetation with N deficiencies.

Additionally, the CDC adjusted to the specific conditions of the experiment was calculated following the methodology proposed by Greenwood et al. (1990) with Eq. 1 fitted to the selected points. For each year and sampling date, the biomass dry weight was compared among the N treatments using one-way ANOVA and the treatment with the highest mean biomass ($P < 0.1$) was selected to determine the relationship between $\%N_c$ and shoot biomass. If more than one treatment resulted in similarly high biomass, the N treatment resulting in the lowest shoot N concentration was selected. If differences among N treatments were not significant, the data from that sampling date were not used. Then, Eq. 1 was fitted to the *%Nc* and *Biomass* selected data by a nonlinear regression iterative procedure and the coefficients were estimated by least-squares.

To build a ground-truth dataset of water status, the leaf conductance was determined by measuring the stomatal conductance of the leaf flag in three representative plants per plots with a clip leaf porometer (Decagon Leaf Porometer, Decagon Devices, Inc. Pullman, WA, USA) within 2 h of local solar noon on May 13th 2019. The leaf porometer measures stomatal conductance by placing the leaf in series with two known conductance elements, and comparing the humidity measurements between them (Sanad et al., 2019). The leaf porometer calculates the stomatal resistance between the inside and outside of the leaf by estimating the flux of water vapor along a diffusion path.

2.3. Spectral and thermal measurements

Canopy reflectance was measured as close as possible to the crop sampling campaigns ensuring cloud-free sky conditions with three hyperspectral sensors: one at ground level and two installed on board a manned aircraft.

Ground-level reflectance spectra were acquired with a portable ASD FieldSpec® Hand-Held VNIR spectroradiometer (Analytical Spectral Devices, Boulder, CO, USA). For each plot, 15 independent spectra, each of these the average of 10 spectra, were randomly acquired 1 m above canopy in a nadir orientation. A reflectance spectrum for each plot was determined as the average of the 15 spectra, and a mean spectrum per treatment was calculated as the average of the four plot replications. The fiber optics provided a 25° field of view with a spectral resolution of 3 nm, resampled to 1 nm over the 325- to 1075-nm wavelength, which resulted in an effective range of 400–900 nm due to noise levels at both ends of the spectrum. Readings were continuously calibrated and optimized by recording the black and baseline reflectance with a Spectralon reference panel (Spectralon, Labsphere Inc., North Sutton, NH, USA) to convert measurements to reflectance values (Quemada and Daughtry, 2016). In each experimental year, three ground-level acquisition campaigns were conducted at the same Zadoks stage as the crop sampling collection: at mid stem elongation, final stem elongation, and flowering (Table 1).

The airborne imagery acquisitions were conducted with a Cessna aircraft flying 300 m above ground and at 70 knots ground speed with heading on the solar plane. The sensors carried by the aircraft were a visible and near infrared (VNIR) hyperspectral imager (Micro-Hyperspec VNIR model, Headwall Photonics, Fitchburg, MA, USA) which collected reflectance in the 400- to 850-nm spectral region with a spectral resolution of 6.5 nm and a spatial resolution of 0.2 m, and a Hyperspec linear-array imager (NIR-100 model, Headwall Photonics, Fitchburg, MA, USA) capturing a portion of the short-wave infrared (SWIR) region from 950 to 1750 nm with 165 spectral bands at 6.05 nm FWHM and 16-bit resolution, yielding 0.6 m spatial resolution. The VNIR and NIR-100 sensor radiometric calibrations were conducted with an integrating sphere (CSTM-USS-2000C LabSphere, North Sutton, NH, USA) using four levels of illumination and six integration times. Hyperspectral imagery was atmospherically corrected measuring incoming irradiance with a field spectrometer and also simulated by the SMARTS model (Gueymard, 1995; Gueymard, 2001). Smoothing of the airborne spectra was performed using the Savitzky-Golay method with a filter length of 9 interpolated to 1 nm. Wavelengths between 1320–1500 and 1085–1185 nm were removed due to atmospheric water vapor absorption (Gao et al., 2009).

RTK coordinates were used to extract the mean spectrum per plot from the hyperspectral imagery, using a 2-m buffer at each side to ensure treatment representativeness. Two airborne campaigns were conducted in 2018: at final stem elongation with the VNIR sensor and at flowering with the VNIR and NIR-100 sensors. Three campaigns were conducted in 2019: at mid stem elongation with the VNIR sensor and at final stem elongation and flowering with the VNIR and NIR-100 sensors (Table 1).

In addition, the aircraft recorded canopy temperature with a thermal camera (SC655 model, FLIR Systems, Wilsonville, OR, USA) with a resolution of 640 × 480 pixels, 16-bit radiometric resolution, 13.1-mm focal length, and 45 × 33.7 °FOV yielding a spatial resolution of 0.25 m. Thermal imagery was calibrated using ground temperature data collected with a handheld infrared thermometer (LaserSight, Optris, Germany) on each flight date. The mean canopy temperature was extracted from each plot with a 2-m buffer to estimate crop water status at flowering in the two years.

2.4. Calculation of hyperspectral and thermal indices

The airborne canopy reflectance and temperature images were used to calculate various commonly used VIs from the literature. The VIs were calculated per plot to analyze the relationships with the crop parameters and the potentials for distinguishing the N and water levels without confounding effects. The VIs were classified according to their main sensitivity to i) canopy structure, ii) chlorophyll $a + b$ and other photosynthetic pigments, iii) canopy N status, and iv) water status (Supplementary material S1). The structural indices are based on the relationship between bands from the NIR and the visible regions. The structural VIs used in this study were the NDVI (Rouse et al., 1973), GNDVI (Gitelson et al., 1996), OSAVI (Rondeaux et al., 1996) and EVI (Huete et al., 2002). The photosynthetic pigment VIs are based on bands from visible and red edge regions, sometimes normalized by the NIR. The photosynthetic pigment VIs used were the PRI (Gamon et al., 1992), CI (Zarco-Tejada et al., 2001:2018), TCARI (Haboudane et al., 2002), DCNI (Chen et al., 2010), mND_{705}, mSR_{705} (Sims and Gamon, 2002), NDRE (Barnes et al., 2000), and $N_{850,1510}$ (Camino et al., 2018).

The "canopy N status indices" comprise VIs that compensate the soil effect by combining a structural and a photosynthetic pigment index, such as in the TCARI normalized by the OSAVI, forming the TCARI/OSAVI index (Haboudane et al., 2002), or in other cases by estimating the two components of the CDC using a planar domain approach (Clarke et al., 2001). The Canopy Chlorophyll Content Index (CCCI) is the most common planar domain index and uses a structural VI as proxy for crop biomass, and a chlorophyll-related VI as proxy for crop N concentration (Barnes et al., 2000; Fitzgerald et al., 2010). The CCCI value of each plot was calculated in a two-dimensional space by representing the NDVI on the X-axis, and NDRE on the Y-axis. Consequently, the value of CCCI was calculated by comparing the distance of each point to the upper and bottom line that involves the cloud of points from the coordinate origin. N-sufficient plots will be located in the graph close to the upper line, whereas N-deficient plots will approach the bottom line.

Two VIs based on the reflectance in the SWIR region ($NDWI_{1240}$ (Gao, 1996) and $NDWI_{1640}$ (Jackson et al., 2004)) were selected to test their ability to determine crop water status, given that they are related to water content (Gao et al., 2015). The SWIR region was not covered by the FieldSpec spectral range and therefore, these NIR/SWIR VIs were calculated only from the aircraft imagery. The accuracy in determining water status using SWIR based VIs was compared against indices based on canopy temperature. The temperature-based indicators used in this study were the canopy-air temperature difference (T_c-T_{air}) (Idso et al., 1977) and the Water Deficit Index (WDI) (Moran et al., 1994). The WDI is an indicator of crop water status that adapts the T_c-T_{air} to partially vegetated fields. To calculate WDI, the Vegetation Index-Temperature (VIT) trapezoid was plotted in a two-dimensional space created by the surface-air temperature differential on the X-axis, and a fractional vegetation cover VI on the Y-axis. As proposed by Moran et al. (1994), the soil-adjusted vegetation index (SAVI; Huete, 1988) was used as a surrogate for the fractional vegetation cover. The VIT trapezoid was defined by two horizontal lines at full ground cover and at bare soil. The value of the full ground cover was the maximum SAVI obtained in all spectral imagery. The bare soil value was the minimum SAVI extracted from 30 pixels randomly located at the pivot-track, half in each water level. The dry and wet bare soil vertices were determined using the image mean temperature of the dry and wet pixels located in the pivot-track of the W1 and W2 zones, respectively. The maximum and minimum water stress vertices at full canopy cover were derived based on the baselines proposed for post-heading winter wheat by Idso (1982). The air vapor water pressure was calculated from the relative humidity and air temperature recorded at the time of image acquisition by the weather station located at the experimental farm. The minimum water stress line of the VIT connects the vertices of wet bare soil and minimum water stress at full canopy cover. Vegetation points close to this line experience minimum water stress. The maximum water stress line links the dry soil vertex with the maximum water stress at full canopy cover. The WDI was calculated for each plot as the ratio between the horizontal distance to maximum and minimum water stress lines.

2.5. Statistical analysis

Statistical analyses were carried out to assess the potential of the different indices for estimating N and water status with low effect from the N-water interaction. In the first step, the structural, photosynthetic pigment and canopy VIs were tested as proxy for N status, and the water indices as proxy for water status. The predictive ability of the VIs to estimate crop status in each sampling campaign was evaluated by calculating the coefficient of determination (R^2) and root mean square error (RMSE) from the linear relationships. The crop parameter used to define the N status was the NNI, calculated from biomass measurements. The crop parameter that described the water status was leaf stomatal conductance (mmol m^{-2} s^{-1}) measured with a leaf porometer. The different water levels were established at flowering stage both years, therefore, the water status was only determined at this stage. In the second step, the indices that best described the NNI and water status were combined using a multiple lineal regression model fitted to the NNI to develop a new index for N status assessment. Finally, the ability of the VIs to distinguish between N levels without confounding effects was evaluated at flowering using the least squares means contrasted with the Tukey test ($P \leq 0.05$) with the N level as the factor. The same methodology was applied to validate the performance for water status but using the water level as the factor for each N level. In addition, a two-way ANOVA was conducted to analyze the effect of N, water and N × Water in the indices. The statistical analyses were conducted with R software (version 4.0.5; R Core Team, 2021).

3. Results

3.1. Crop response to water and nitrogen supply

Different climatic conditions between experimental years, particularly rainfall distribution, had a large effect on crop growth. The total amount of water received by W2 plots until biomass collection at flowering stage was 304 mm in 2018 and 216 mm in 2019. Differences in water availability between experimental years were also observed at tillering and stem elongation (Fig. 2). Since no water was available for irrigation for several weeks of the 2019 growing season, the wheat suffered severe water stress, which later limited the crop response to N supply. Biomass accumulation and %N (Table 2) were greatly affected by the different climatic conditions, widening the range in the crop variables investigated and creating a suitable dataset for testing the relationships between crop performance and spectral measurements.

Shoot biomass increased with growth stages and %N decreased (Table 2). This N dilution effect was also observed when comparing the crop parameters between years; the biomass accumulation tended to be higher in 2018, with significant differences between years at mid stem elongation and flowering ($P \leq 0.05$). In contrast, the %N was higher in 2019 with significant differences between years in the same dates as biomass. The effect of the different N fertilization rates was observed in the relative position with the CDC: data from low N levels remained below the critical requirements, whereas high N levels tended to approach or surpass the $\%N_c$ (Fig. 3a).

Increasing N levels had a positive effect on biomass, %N and NNI in the two experimental years (Table 2). The NNI distinguished between N-deficit plots (N0 and N1), plots with the recommended rate (N2), and the overfertilized plots (N3) in all the 2018 GSs. The NNI distinguished between the nonfertilized plots and the overfertilized plots in all the 2019 GSs, but the discriminatory capacity of intermediate N levels varied with the GS. Treatments N1 and N2 had a similar NNI at mid stem elongation in 2019, but a different NNI at final stem elongation. At flowering, NNI differences between N1 and N2 treatments were clearer in the W2 level than in the W1 (Table 2). Differences in the NNI between the water levels established in each N level were only found in the 2019 N2 treatment, yielding higher a NNI in the W2 plots. The effect of water levels was clear in reducing %N in the N2 and N3 treatments but was also accompanied by a reduction in biomass. Increasing water level was associated with an increase in the spikes' N content (kg N ha^{-1}): it was 12 % higher in W2 than in W1 in 2018 and 9% higher in N3-W2 plots

Table 2
Biomass (kg DM ha^{-1}), N concentration (N conc, %), Nitrogen Nutrition Index (NNI) and flag leaf conductance (mmol m^{-2} s^{-1}) for the various N and water levels at different Zadoks stages for the two experimental years. Within a year and growth stage, values followed by the same letter are not significantly different according to Tukey's test at $P \leq 0.05$.

	Treatment		2018			2019			
	Water	N	Biomass (kg DM ha^{-1})	N conc. (%)	NNI	Biomass (kg DM ha^{-1})	N conc. (%)	NNI	Conductance (mmol m^{-2} s^{-1})
Mid stem elongation		N0	1568 a	2.46 a	0.55 a	1521 a	2.83 a	0.63 a	–
		N1	2091 a	2.63 a	0.68 a	1683 a	3.23 ab	0.74 ab	–
		N2	2843 b	3.00 a	0.88 b	1531 a	3.58 bc	0.8 bc	–
		N3	3322 b	3.96 b	1.25 c	1771 a	3.70 c	0.89 c	–
Final stem elongation		N0	4256 a	1.04 a	0.37 a	4068 a	1.48 a	0.53 a	–
		N1	5924 a	1.14 a	0.47 a	5107 ab	1.65 ab	0.58 a	–
		N2	8242 b	1.68 b	0.79 b	6456 bc	1.85 bc	0.78 b	–
		N3	8593 b	2.29 c	1.1 c	7456 c	2.00 c	0.9 b	–
Flowering	W1	N0	8108 a	0.69 a	0.33 a	6576 a	0.94 a	0.4 a	144 ab
		N1	9830 ab	0.8 ab	0.41 a	9667 ab	1.12 abc	0.57 ab	151 ab
		N2	12,965 c	1.06 bc	0.61 b	9970 ab	1.17 abc	0.6 bc	175 abc
		N3	11,851 bc	1.51 e	0.84 c	10,551 b	1.56 d	0.83 d	141 a
	W2	N0	8797 a	0.69 a	0.33 a	7412 a	0.92 a	0.41 a	297 d
		N1	11,101 abc	0.8 ab	0.43 a	9487 ab	1.12 ab	0.56 ab	245 cd
		N2	12,979 c	1.14 cd	0.66 b	10,877 b	1.37 cd	0.74 cd	240 cd
		N3	13,713 c	1.40 de	0.83 c	11,654 b	1.36 bcd	0.75 d	266 cd

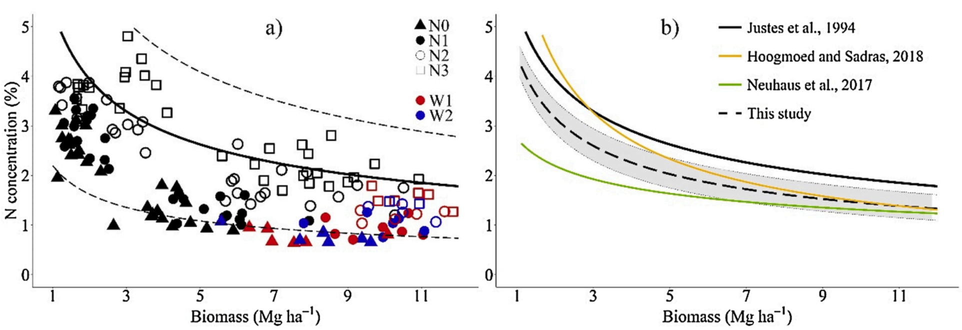

Fig. 3. a) Pair values of aerial biomass (Mg ha^{-1}) and N concentration (%) for all N levels (symbols), water levels (colors) and sampling dates of the experiment. The continuous line is the critical N dilution curve (CDC) ($\%N_c = 5.35$ x Biomass $^{-0.442}$) for winter wheat, and the dashed lines the envelop curves ($N_{max} = 8.3$ x Biomass $^{-0.442}$ and $N_{min} = 2.2$ x Biomass $^{-0.442}$) according to Justes et al. (1994). b) Comparison of the CDC proposed by Justes et al. (1994) (solid black line) with the CDC fitted to the N2 treatments in this study ($\%N_c = 4.42$ x Biomass $^{-0.483}$, $R^2 = 0.88$) (dashed line); the gray area indicates the envelop curves at 95 % confidence intervals ($N_{max} = 4.14$ x Biomass $^{-0.532}$ and $N_{min} = 4.73$ x Biomass $^{-0.433}$). The green line is the CDC under water limited conditions proposed by Neuhaus et *al.* (2017) ($\%N_c = 0.7 \times 3.91$ x Biomass $^{-0.32}$), and the yellow line the CDC proposed by Hoogmoed and Sadras (2018) ($\%N_c = 6.75$ x Biomass $^{-0.66}$).

with respect to N3-W1 in 2019 (data not shown).

A strong crop response to water levels was observed in the leaf conductance measured at flowering in 2019 (Table 2). Treatments with a higher irrigation level showed higher conductance than treatments with lower water application across all the N levels ($P \leq 0.05$). For each water level, no differences in leaf conductance were observed between N levels. The greatest difference between water levels was observed in N0, which obtained the highest leaf stomatal conductance mean value among the W2 plots.

Table 3
Coefficient of determination (R^2) of the linear relationship between Nitrogen Nutrition Index (NNI) and the different spectral vegetation indices extracted from the airborne imagery (AB) and the ground-level FieldSpec (FS). Bold numbers were significant at $P \leq 0.001$.

Spectral indices	Mid stem elongation			Final stem elongation				Flowering			
	2018	2019		2018		2019		2018		2019	
	FS	AB	FS	AB	FS	AB	FS	AB	FS	AB	FS
NDVI	**0.51**	0.02	0.10	**0.53**	**0.41**	**0.52**	**0.39**	**0.59**	**0.59**	**0.40**	**0.41**
GNDVI	**0.50**	0	0.20	**0.57**	**0.54**	**0.54**	**0.51**	**0.62**	0.48	**0.52**	**0.49**
OSAVI	**0.53**	0.03	0.11	**0.60**	**0.53**	**0.56**	**0.41**	**0.65**	0.46	**0.39**	**0.41**
EVI	**0.54**	0.03	0.11	**0.65**	**0.59**	**0.57**	**0.43**	**0.68**	0.33	**0.38**	**0.39**
PRI	**0.52**	0.02	0.15	**0.59**	**0.61**	0.28	**0.51**	**0.61**	**0.59**	0.27	0.28
CI	**0.48**	0	0.20	**0.58**	**0.67**	**0.59**	**0.53**	**0.65**	**0.63**	**0.40**	**0.42**
TCARI	**0.30**	0.27	0.10	0.26	**0.48**	0.35	0.44	0.20	0.20	0.16	0.42
DCNI	**0.45**	**0.40**	0.22	0.28	**0.69**	**0.46**	**0.59**	**0.42**	**0.61**	**0.42**	**0.49**
mND_{705}	**0.53**	0.02	0.22	**0.56**	**0.58**	**0.62**	**0.60**	**0.64**	**0.63**	**0.38**	**0.45**
mSR_{705}	**0.48**	0.02	0.22	**0.58**	**0.69**	**0.62**	**0.55**	**0.64**	**0.62**	**0.38**	**0.40**
NDRE	**0.51**	0.07	0.27	**0.57**	**0.64**	**0.58**	**0.64**	**0.65**	**0.66**	**0.50**	**0.51**
$N_{850,\ 1510}$	–	–	–	–	–	0.31	–	**0.45**	–	0.18	–
TCARI/OSAVI	**0.46**	**0.39**	0.25	**0.46**	**0.57**	**0.53**	**0.64**	**0.56**	0.51	**0.59**	**0.58**
CCCI	**0.50**	**0.56**	**0.44**	**0.54**	**0.67**	**0.53**	**0.73**	**0.64**	**0.65**	**0.62**	**0.59**

3.2. Vegetation indices as proxy of NNI across growth stages

Most of the VIs based on the red edge region had a significant relationship with the NNI, showing variations in R^2 and RMSE according to the various GSs and sensors (Table 3 and Supplementary material S2). The NDRE index, based on red edge and NIR reflectance, yielded $R^2 >$ 0.5 with the NNI in most cases, except for mid stem elongation 2019. The suitability of the red edge region as an N status indicator was also supported by the performance of other photosynthetic pigment VIs based on reflectance in red edge and visible regions: the DCNI, mND_{705} and mSR_{705}. Also, the CI, which used two wavelengths to calculate the slope of the red edge region, was related to the NNI and behaved similarly to mSR_{705}: the difference in RMSE between the two VIs was less than 0.006 in all cases (Supplementary material S2). Additionally, the PRI, based only on reflectance from the visible (or the pigment absorption region) presented a high R^2 value with the NNI, but its performance varied widely between acquisition dates. In this study, the VI based on the NIR-SWIR bands ($N_{850,\ 1510}$) showed a weak correlation with the NNI, as well as the TCARI.

The suitability of the red edge region combined with NIR to estimate NNI is supported when observing the better performance of NDRE with respect to the structural VIs NDVI and GNDVI in almost all cases. Structural VIs are calculated with an equation similar to NDRE but switching red edge reflectance by red or green. Among them, the GNDVI performed better than the NDVI at final stem elongation with the two sensors for both years, especially with the FieldSpec. When analyzing the EVI, which was calculated with the same wavelengths as the NDVI but adding blue reflectance, it was observed that the airborne data obtained a higher R^2 and lower RMSE than the FieldSpec in most cases; also, the correlation enhanced with respect to the NDVI at mid stem elongation 2018 and final stem elongation both years. Similarly, the OSAVI, which was calculated with the same wavelengths as the NDVI but adding a factor, performed better than the NDVI the same dates as the EVI.

Overall, the best correlation with the NNI was obtained with the canopy indices, as the R^2 were among the highest in all stages. Particularly, the CCCI was the only index that reached $R^2 > 0.72$ in one of the sampling campaigns (Table 3). The low R^2 of most VIs at mid stem elongation 2019 was attributed to the effects caused by the soil background at low ground cover stages. This effect was compensated with the canopy VIs, especially with the CCCI, supporting the suitability of the planar domain VIs to remove the soil background influence. At mid stem elongation 2018 most VIs performed similarly ($R^2 \sim 0.5$) and no improvement was achieved with the canopy indices because the amount of biomass was higher than at mid stem elongation 2019 (Table 2). Most structural and photosynthetic pigment VIs performed poorly at flowering 2019, suggesting that they were inaccurate under water stress. This was particularly evident with the PRI with the two sensors.

The CCCI showed a significant correlation with the NNI when calculated with the aircraft or FieldSpec in all stages. In this study, the CCCI calculated with the two hyperspectral sensors behaved similarly: they were significantly correlated in all dates ($P \leq 0.001$) with a $R^2 = 0.64$ ($P \leq 0.001$) when all dates are analyzed together (Supplementary material S3). The equations of the upper ($NDRE_{max}$) and lower ($NDRE_{min}$) lines that involved the data from both campaigns were similar with the two sensors (Fig. 4) and with the equations reported by Fitzgerald et al. (2010) for winter wheat in Australia ($NDRE_{max} = 0.61 \times NDVI$; $NDRE_{min} = 0.34 \times NDVI$), who also used a FieldSpec.

3.3. Spectral analysis at different water levels to assess leaf conductance

The effect of the water levels on the reflectance spectra was consistently detected in the SWIR as a function of different N rates (Fig. 5). As expected, low water availability increased the spectral reflectance in the regions centered at 1240 nm and 1640 nm. Smaller differences in the NIR reflectance appeared in most cases. In the visible region, differences in the red region were evident, detected for all N levels in 2019 and for N0 in 2018. For this reason, the normalized difference between the NIR and SWIR, proposed by Gao et al. (2015) was tested to detect crop water status.

The distribution of all observations at flowering in the VIT plotted in the two dimensional space formed by the SAVI and the temperature difference obtained from the thermal camera clearly distinguished among data from W1 and W2 water levels in both experimental years (Fig. 6). The location in the VIT also stated that the water stress suffered by all plots was lower in 2018 than in 2019, with significant differences in the WDI between years ($P \leq 0.05$), in agreement with comments above on climate conditions.

Ground-based measurements of leaf stomatal conductance were better correlated with the WDI than with canopy-air temperature differences (Table 4), supporting the improvement of the crop water status estimation when canopy temperature is corrected by the ground cover (Fig. 7). The relationship of VIs based on SWIR reflectance with leaf stomatal conductance was significant only for $NDWI_{1640}$ ($P \leq 0.001$), but the $R^2 < 0.34$ for both indices (Table 4). The trend of the linear relationships between the index related to water stress (WDI) and the indices related to water content ($NDWI_{1240}$, $NDWI_{1640}$) were negative

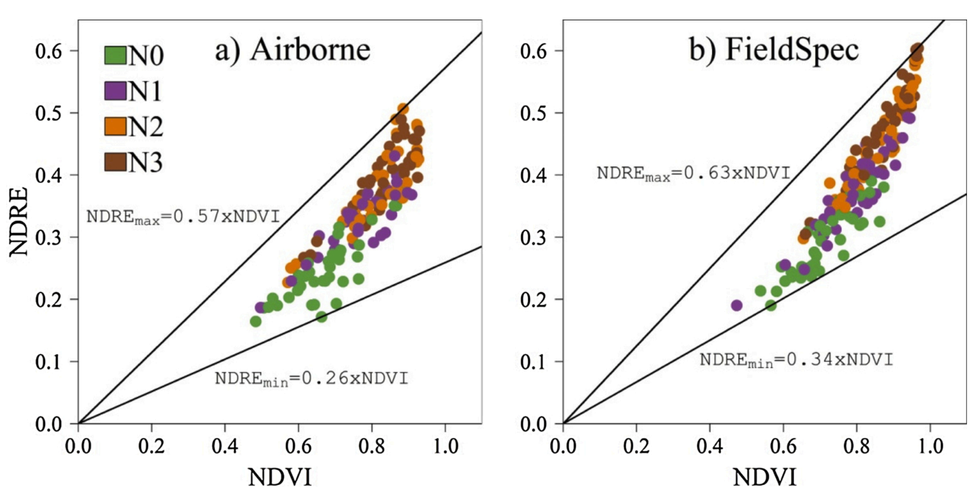

Fig. 4. Graphical representation of the Canopy Chlorophyll Content Index (CCCI) developed with the mean value of the NDVI and NDRE of each plot extracted from a) the airborne imagery and b) with the FieldSpec in all remote sensing campaigns. The CCCI value of each plot with a certain NDVI was calculated as $CCCI = (NDRE - NDRE_{min})/(NDRE_{max} - NDRE_{min})$.

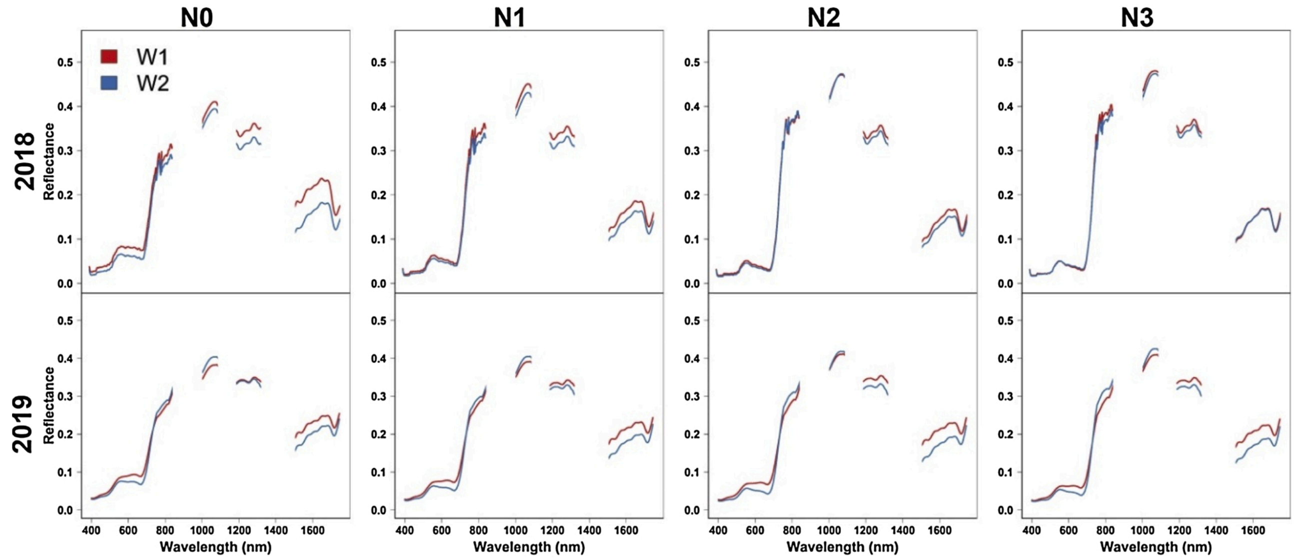

Fig. 5. Average canopy reflectance acquired with the airborne hyperspectral sensors in the 400-1750 nm region at 300 m above ground level at flowering separated by N and water levels each year.

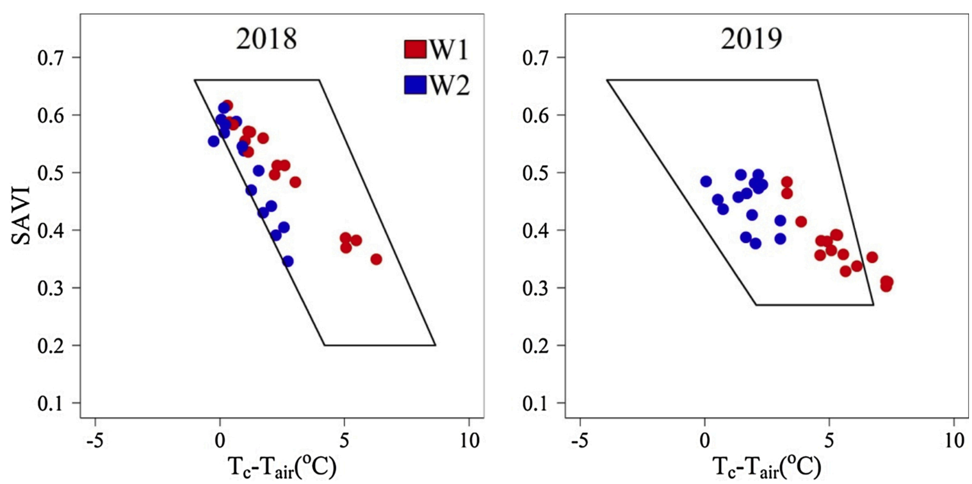

Fig. 6. Representation of all observations at flowering in the Vegetation Index-Temperature (VIT) trapezoid plotted in the two dimensional space formed by the soil adjusted vegetation index (SAVI) and the difference between canopy (T_c) and air temperature (T_{air}). Symbols are the mean value for each plot.

Table 4
Coefficient of determination (R^2) and root mean square error (RMSE) of the linear relationship between leaf conductance (mmol m^{-2} s^{-1}) and Water Deficit Index (WDI) with different spectral and temperature-based indices extracted from the airborne imagery at flowering 2019. Bold numbers indicate significance level $P \leq 0.001$.

	Conductance		WDI	
	R^2	RMSE (mmol m^{-2} s^{-1})	R^2	RMSE
WDI	**0.66**	**39.56**	–	–
T_c-T_{air}	**0.59**	**43.26**	–	–
$NDWI_{1240}$	0.31	56.20	**0.56**	**0.175**
$NDWI_{1640}$	**0.34**	**54.76**	**0.63**	**0.162**

with a $R^2 > 0.55$ when indices were extracted from the airborne spectra. Between them, the best correlation was obtained with the $NDWI_{1640}$ ($R^2 = 0.63$). In addition, the $NDWI_{1640}$ was the only VI based on SWIR bands that found differences in water status between years ($P \leq 0.05$). Therefore, the optical indices involving SWIR bands were able to detect water status, but the best indicator of crop water status was the WDI.

3.4. Development of a N status indicator combining N and water indices

The best hyperspectral VI for the NNI (CCCI) and temperature-based indicator for water status (WDI) were combined using a multiple lineal regression model to develop a new indicator for N status monitoring (Fig. 8). The assessment capacity was enhanced when the NNI was estimated based on the CCCI and WDI rather than only on the CCCI alone, as the R^2 increased and the RMSE was reduced. When analyzing each year individually, a similar performance in the assessment capacity was obtained at flowering 2018 (RMSE = 0.123 and $R^2 = 0.64$ for the CCCI versus RMSE = 0.127 and $R^2 = 0.62$ for *f*(CCCI, WDI)), and substantial improvement was achieved at flowering 2019, the year that the crop experienced a more severe water stress (RMSE = 0.091 and $R^2 = 0.62$ for CCCI versus RMSE = 0.081 and $R^2 = 0.70$ for *f*(CCCI, WDI)).

The effect of the N and water levels in the VIs and the temperature-based indicators was tested using the aircraft imagery acquired at flowering for both years (Fig. 9 and Supplementary material S4, S5). Most VIs distinguished between N-deficit (N0 and N1) and N-sufficient plots (N2 and N3); nevertheless, the CCCI also distinguished between the nonfertilized plots (N0) and the plots with the reduced dose (N1), as well

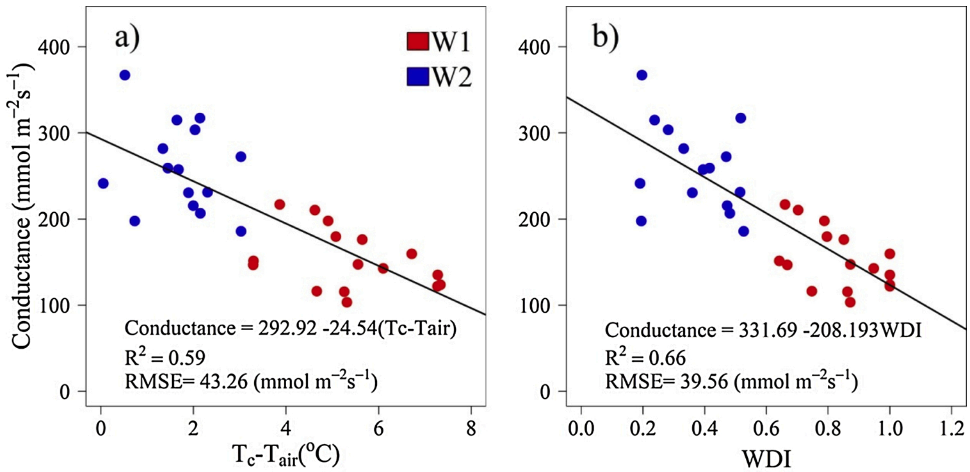

Fig. 7. Pair values of leaf stomatal conductance (mmol m^{-2} s^{-1}) and a) canopy-air temperature difference (T_c - T_{air}) or b) the Water Deficit Index (WDI) extracted from the airborne imagery at flowering 2019 (symbols). Blue symbols are the pair values from plots that were irrigated at flowering (W2) and red symbols pair values of plots not irrigated at flowering (W1). The solid lines are the linear regression with the corresponding equation, coefficient of determination (R^2) and root mean square error (RMSE).

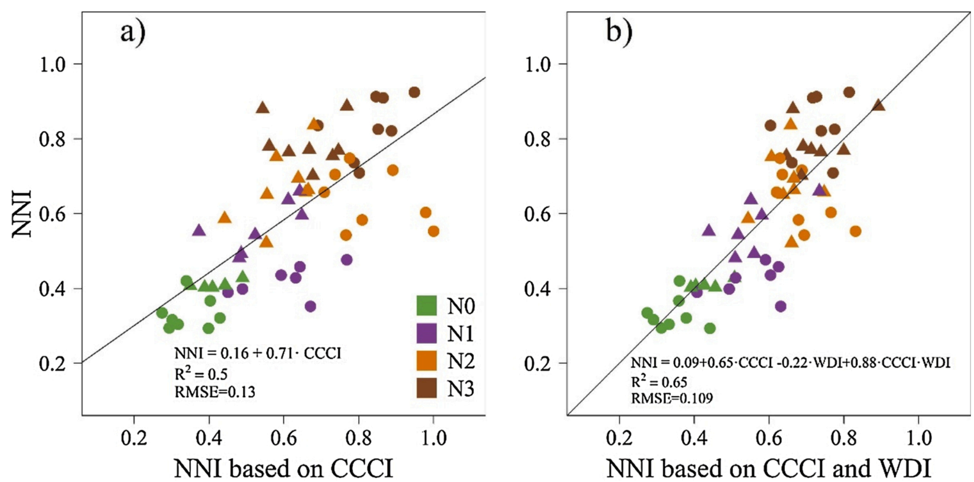

Fig. 8. The NNI observed versus the estimated NNI based on a linear relationship based on a) the CCCI and b) a combination of the CCCI and WDI. Symbols are the pair values for the various N treatments, circles for 2018 and triangles for 2019. The solid lines are the linear regression with the corresponding equations, coefficient of determination (R^2) and root mean square error (RMSE).

as between the N1 and N3 plots. The new index based on spectral and thermal information performed similarly to the CCCI when identifying N levels. The ANOVA test indicated that all spectral VIs were highly affected by N fertilization ($P \leq 0.001$), except the TCARI (Supplementary material S4). The capacity of NNI and *f*(CCCI,WDI) to distinguish between the N levels within the W2 plots was similar: both indicators distinguished between N1 and N2 plots and identified the N-deficit (N0 and N1) and N-sufficient (N2 and N3) treatments at flowering both years.

As water availability was similar in W1 and W2 in 2018, the VIs behaved similarly in both water levels; however, differences in water availability in W1 and W2 caused differences in VI behaviour between water levels in 2019 (Supplementary material S4). That year, the structural and photosynthetic pigment VIs at W1 and W2 were different for most N levels, showing that these indices were sensitive to the water effect. However, the canopy VIs reduced these differences across all N levels; most particularly differences in the CCCI between water levels were significant only for N0 in 2019 (Fig. 9b). No differences in *f*(CCCI, WDI) between water levels were found in any N level and year (Fig. 9e, f) showing the robustness of the new indicator in estimating crop N status under different water stress conditions. In addition, the ANOVA test indicated that all spectral indices were affected by the water levels at the 0.001 probability level, whereas the CCCI was at 0.05 and *f*(CCCI, WDI) was the only index not affected (Supplementary material S4).

Differences between water levels in 2018 were only detected with information retrieved from thermal imagery (Supplementary material S4, S5). The WDI quantified the water status with a reduced effect of the N levels, showing that for W2 all N levels in the same year suffered a similar water stress, whereas, for W1 the water stress was higher for N0 and decreased with increasing N level, especially in 2018 (Fig. 9c, d). Compared to the canopy-air temperature difference, the WDI increased the differences between water levels and mitigated the effect of the N levels (Supplementary material S5). This was particularly evident in the N0 level, in which the high temperature associated with higher soil exposure but not with lower water availability was compensated by the WDI. The two VIs based on SWIR reflectance behaved similarly when identifying water and N levels; they distinguished between the water levels established in each N level in 2019, but in 2018, they displayed differences between N levels but not between water levels. These results emphasize that the WDI was the most reliable indicator to determine crop water stress with a minimum effect of N status.

The robustness of the CCCI for estimating N levels under various water conditions was evident in the CCCI map obtained by the airborne hyperspectral imagery both in 2018 and 2019 (Fig. 10). No differences in the CCCI were observed between the W1 and W2 areas with equal N application, whereas the N levels were easily identifiable in both water levels (in agreement with Fig. 9a, b). On the other hand, the WDI was particularly sensitive to crop water status, and even in 2018 was able to

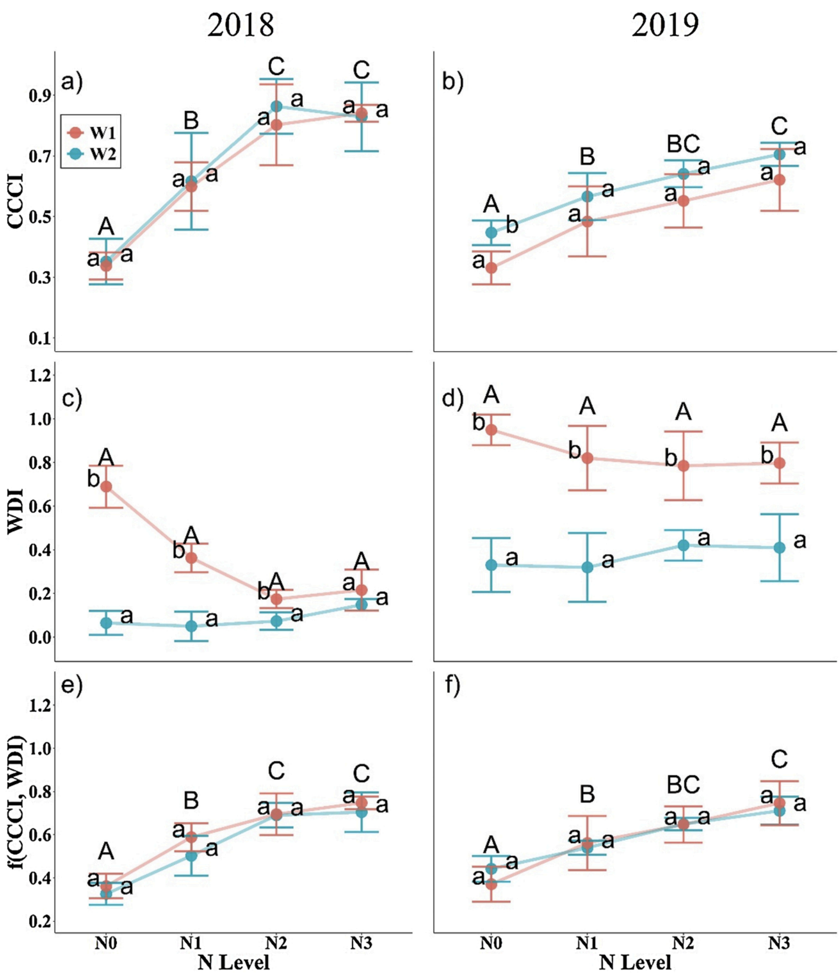

Fig. 9. Canopy Chlorophyll Content Index (CCCI), Water Deficit Index (WDI) and the new combined indicator proposed for N status assessment retrieved from the aircraft imagery for each N and water level (W1 and W2) at flowering in both experimental years. Symbols are mean values and bars standard errors. Capital letters above the error bars indicate differences among N levels and lower case letters next to the means indicate differences between water levels in each N level according to Tukey test 95 %.

distinguish between the W1 and W2 sectors of the field experiment. The effect of N on the WDI map was relatively minor compared to the influence of the water level (in agreement with Fig. 9c, d).

4. Discussion

This study confirmed the difficulty of disentangling crop N and water status using only spectral information, as the confounding effect was evident in the spectra. Determining the cause of the stress suffered by the crop is a key issue for guiding fertilization and water management (Gonzalez-Dugo et al., 2009). The NNI was a reliable indicator of crop N status and proved to be robust under different water levels, even if %N in shoots decreased in well fertilized treatments with lower water availability. However, the CDC fitted to the data from this study showed that the $\%N_c$ was lower than the reference values proposed by Justes et al. (1994) for winter wheat under no water limitation (Fig. 3b). Because of that, the NNI values were low even for the well fertilized plots (N2 treatments; Table 2). Similar results were reported for the CDC curves obtained under water-limited conditions in Australia (Neuhaus et al., 2017; Hoogmoed and Sadras, 2018) leading to Hoogmoed and Sadras (2018) to hypothesize that water-limited crops exhibit lower N uptake than well-watered crops and may require specific $\%N_c$ values. The $\%N_c$ proposed by these curves lay within the 95 % confidence interval of our CDC when biomass > 4.5 Mg DM ha^{-1} (Fig. 3b). Nevertheless, more research is needed to clarify if the lower *%Nc* values reported are due to water limited conditions and to solve the discrepancies in the *%Nc* at biomass < 4 Mg DM ha^{-1}. This issue is highly relevant, as we hypothesize that using the CDC obtained for winter wheat under no water limitation could lead to overfertilization in water limited environments.

In this study we propose the use of different remote sensing indices based on spectral and thermal information to determine the N and water status separately and therefore, to adjust N fertilization and irrigation according to crop demands. However, certain limitations were observed when applying most VIs based on spectral information: i) they were highly affected by the soil background signal at early crop growth stages, when decisions on N fertilization application are made, ii) their performance was reduced when the crop experienced water stress, and iii) the value of the indices decreased when the crop suffered from N or water stress, making it difficult to identify the reason behind the crop deficiencies. This study demonstrated that these limitations can be overcome by simultaneous analyses of the CCCI and WDI.

In this regard, the CCCI, which relates a structural and a chlorophyll index, showed a robust and consistent correlation with the NNI within a wide range of ground cover and water status when canopy reflectance was measured at ground level or 300 m above the experiment. These results are in agreement with Fitzgerald et al. (2010), who obtained good CCCI performance at estimating crop N status in winter wheat, and with El-Shikha et al. (2007) and Bronson et al. (2017), who reported the low effect of crop water status on the CCCI. The good match between the lines used to calculate the CCCI in this experiment and in Fitzgerald et al. (2010) provides new insight for the normalization of the equations.

Our study validated the use of the WDI to estimate water status and pointed out the convenience of compensating canopy temperature by the ground cover to isolate the plant signal. The WDI correction had more effect in the areas with low ground cover, in which the thermal difference between air and dry soil > 8 °C. It is well known that the amount of water needed to supply crop demand increases with biomass (Tanner and Sinclair, 1983), but in this experiment the WDI suggested

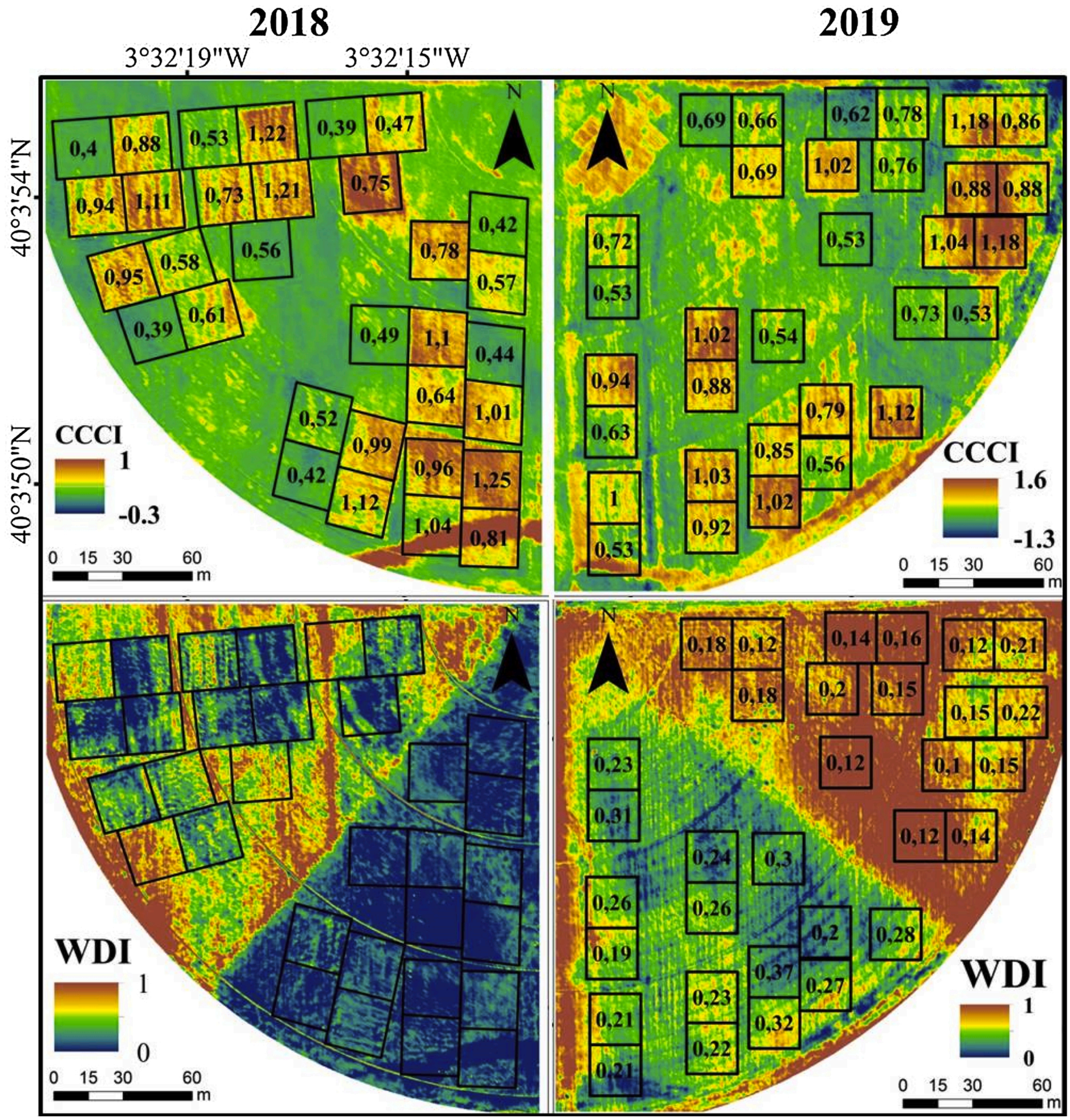

Fig. 10. Canopy Chlorophyll Content Index (CCCI) and Water Deficit Index (WDI) maps retrieved from a hyperspectral and a thermal imager on-board an aircraft at the flowering stage of both experimental years. Plot values in the CCCI and WDI maps represent the Nitrogen Nutrition Index (NNI) and leaf conductance (mmol m^{-2} s^{-1}), respectively (no data available for WDI 2018).

that N0 plots were the most water stressed, even though the amount of water received was the same as the plots with more biomass. Several reasons could explain this apparent contradiction. Seligman et al. (1983) indicated that N deficit plants increase leaf temperature because the biological processes to maturity are accelerated. This effect was also reported in other studies (Heitholt et al., 1991; Tilling et al., 2007; Fois et al., 2009; Mon et al., 2016). Additionally, in N-deficient cereals of semiarid environments it was reported that a moderate increase in N supply enhances WUE (Cossani et al., 2012). Finally, the proof that it is necessary to correct the effect of N fertilization or biomass in thermal indices is that the leaf stomatal conductance was better correlated with the WDI than with the thermal difference (T_c-T_{air}). In agreement with these results, field studies showed that variable-rate irrigation based on maps of planar indices such as the WDI could greatly enhance WUE (O'Shaughnessy et al., 2015). In this study, the thermal camera was the only sensor that detected differences between water levels in 2018; the non-limited water scenario.

This study reported that the sensitivity of the CCCI to winter wheat N status increased when it was combined with the temperature-based indicator (WDI), because this combination mitigated the effect of the crop water status. These results led us to propose a new indicator for N status monitoring by combining spectral and thermal information. Similarly, Quemada et al. (2014) reported better grain yield prediction in maize when spectral and thermal information was combined. It is well known that the NNI and grain yield are correlated and affected by N and water availability (Sadras and Lemaire, 2014). To ensure that the crop uptakes the applied N and to mitigate N losses to the environment, the water status of the crop has to be considered before N fertilization (Quemada and Gabriel, 2016). For field application of the proposed method, it is advised to simultaneously measure reflectance in the VNIR region and canopy temperature to provide a map of the CCCI and WDI to calculate the proposed N status-related index as *f*(CCCI,WDI). In irrigated fields with the option of variable water delivery, irrigation should be applied in areas with a high WDI that do not experience N deficit (high CCCI and *f*(CCCI,WDI)) because the possibility of enhancing crop growth is higher. In contrast, areas with a high WDI in which N is a relevant limiting factor would be less likely to profit from the additional water applied and the risk of diminishing water use efficiency would be higher. The areas in which applied N will be prone to N uptake will be those with a low *f*(CCCI,WDI) and a low WDI, indicating that the area experiences N deficit and has sufficient water availability (Zillmann et al., 2006; Tilling et al., 2007). In contrast, N applications should be avoided in water-limited areas (i.e. a low *f*(CCCI,WDI) with a high WDI) as the crop would likely not use the N applied and the risk of increasing losses would be higher. Similarly, a high CCCI or *f*(CCCI, WDI) areas should not receive N fertilization given that the crop N deficit is low. Besides multiple linear regression, the spectral and thermal information could be used by emerging machine learning techniques based on ensemble methods (i.e. random forest, neuronal networks) that already showed potential in obtaining robust outcomes from the combination of multiple variables in agri-environmental studies (Mutanga et al., 2012; Lebourgeois et al., 2017).

Using two different airborne sensors simultaneously (i.e. covering the VNIR + thermal regions) is more complex than when one camera is used (e.g. collecting imagery with a VNIR camera only) due to the different spatial resolutions obtained and co-registration issues between non-aligned detectors. Nevertheless, this study and others clearly demonstrate the need for acquiring imagery covering the VNIR portion of the electromagnetic spectrum where photosynthetic pigments can be quantified due to their link with nutrient status, and the spectral region more directly related with canopy transpiration for its direct connection with water status and water stress detection. New multispectral cameras are becoming available which can be installed on board manned and unmanned vehicles which acquire images with co-registered detectors covering the VNIR and thermal infrared regions, overcoming some of the issues indicated above.

The proposed approach is an application of the N and water co-limitation concept (Sadras, 2004; Cossani and Sadras, 2018). Because of the empirical basis of the proposed indicators, their reliability for improving N fertilization and water management should be tested in different cultivars, soils, and climate conditions.

5. Conclusion

The confounding effect of crop N and water status in the spectral reflectance was evident and the results of this study point out the difficulty of using only reflectance-based vegetation indices to discriminate between N and water stress. This limitation can be overcome by combining spectral reflectance with canopy thermal information to accurately adjust N fertilization and irrigation to crop requirements. The reliability of the WDI in estimating water status was demonstrated in this study, because the WDI correlated with leaf stomatal conductance and showed robustness at detecting irrigation levels while reducing the influence of soil background. The best VI to assess crop N status was the CCCI, which presented significant relationship with the NNI in all cases, even at early stages when the CCCI compensated for soil background effect. The CCCI distinguished between N fertilization levels and it was only slightly affected by crop water status. The effect of water status on the CCCI was mitigated when it was combined with the WDI to provide a robust indicator (*f*(CCCI, WDI)) that identified N levels regardless of the water regime. The RMSE of assessing the NNI was reduced from 0.130 when based on the CCCI to 0.109 when based on *f*(CCCI, WDI). This study demonstrates that simultaneous analysis of CCCI and WDI data derived from remote sensing technology may greatly contribute to site-specific adjustment of N fertilization and irrigation; however, the robustness of the indicators must be tested in different environments and cultivars.

CRediT authorship contribution statement

J.L. Pancorbo: Conceptualization, Methodology, Investigation, Writing - original draft, Visualization. **C. Camino:** Methodology, Investigation, Writing - review & editing. **M. Alonso-Ayuso:** Investigation, Writing - review & editing. **M.D. Raya-Sereno:** Investigation, Writing - review & editing. **I. Gonzalez-Fernandez:** Investigation, Writing - review & editing. **J.L. Gabriel:** Investigation, Writing - review & editing. **P.J. Zarco-Tejada:** Methodology, Investigation, Writing - review & editing. **M. Quemada:** Conceptualization, Methodology, Investigation, Writing - review & editing, Project administration, Funding acquisition, Supervision.

Declaration of Competing Interest

None.

Acknowledgements

This work was funded by the Ministerio de Economía y Competitividad (Spain; AGL2017-83283-C2-1-R; PRE2018-084215) and Ministerio de Educación (Spain; FPU17/01251). Comunidad de Madrid, Spain (AGRISOST-CM S2018/BAA-4330 project) and Structural Funds 2014-2020 (ERDF and ESF). We thank the staff from La Chimenea research station (IMIDRA) for their technical support, Javier López Llorens for his laboratory work, and QuantaLab-IAS-CSIC staff members A. Hornero, A. Vera, D. Notario, and R. Romero for airborne and laboratory assistance.

Appendix A. Supplementary data

Supplementary data associated with this article can be found, in the online version, at https://doi.org/10.1016/j.eja.2021.126287.

References

Aguilera, E., Lassaletta, L., Sanz-Cobena, A., Garnier, J., Vallejo, A., 2013. The potential of organic fertilizers and water management to reduce N_2O emissions in Mediterranean climate cropping systems. A review. Agric. Ecosyst. Environ. 164, 32–52. https://doi.org/10.1016/j.agee.2012.09.006.

Angus, J., Fischer, R.A., 1991. Grain protein responses to nitrogen applied to wheat growing on a red earth. Aust. J. Agric. Res. 42, 735–746. https://doi.org/10.1071/AR9910735.

Arregui, L.M., Lasa, B., Lafarga, A., Irañeta, I., Baroja, E., Quemada, M., 2006. Evaluation of chlorophyll meters as tools for N fertilization in winter wheat under humid Mediterranean conditions. Eur. J. Agron. 24, 140–148. https://doi.org/10.1016/j.eja.2005.05.005.

Barnes, E.M., Clarke, T.R., Richards, S.E., Colaizzi, P.D., Haberland, J., Kostrzewski, M., Aller, P., Choi, C., Riley, E., Thompson, T., Lascano, R.J., 2000. Coincident detection of crop water stress, nitrogen status and canopy density using ground based multispectral data. Proc. Fifth Int. Conf. Precis. Agric. 1619.

Basso, B., Cammarano, D., Grace, P.R., Cafiero, G., Sartori, L., Pisante, M., Landi, G., de Franchi, S., Basso, F., 2009. Criteria for selecting optimal nitrogen fertilizer rates for precision agriculture. Ital. J. Agron. 4, 147–158. https://doi.org/10.4081/ija.2009.4.147.

Bronson, K.F., White, J.W., Conley, M.M., Hunsaker, D.J., Thorp, K.R., French, A.N., Mackey, B.E., Holland, K.H., 2017. Active optical sensors in irrigated durum wheat: nitrogen and water effects. Agron. J. 109, 1060–1071. https://doi.org/10.2134/agronj2016.07.0390.

Camino, C., González-Dugo, V., Hernández, P., Sillero, J.C., Zarco-Tejada, P.J., 2018. Improved nitrogen retrievals with airborne-derived fluorescence and plant traits quantified from VNIR-SWIR hyperspectral imagery in the context of precision agriculture. Int. J. Appl. Earth Obs. Geoinf. 70, 105–117. https://doi.org/10.1016/j.jag.2018.04.013.

Chen, D., Huang, J., Jackson, T.J., 2005. Vegetation water content estimation for corn and soybeans using spectral indices derived from MODIS near- and short-wave infrared bands. Remote Sens. Environ. 98, 225–236. https://doi.org/10.1016/j.rse.2005.07.008.

Chen, P., Haboudane, D., Tremblay, N., Wang, J., Vigneault, P., Li, B., 2010. New spectral indicator assessing the efficiency of crop nitrogen treatment in corn and wheat. Remote Sens. Environ. 114, 1987–1997. https://doi.org/10.1016/j.rse.2010.04.006.

Clarke, T.R., Moran, M.S., Barnes, E.M., Pinter, P.J., Qi, J., 2001. Planar domain indices: a method for measuring a quality of a single component in two-component pixels. Int. Geosci. Remote Sens. Symp. 3, 1279–1281. https://doi.org/10.1109/igarss.2001.976818.

Cossani, C.M., Sadras, V.O., 2018. Water–Nitrogen colimitation in grain crops. Adv. Agron. 150, 231–274. https://doi.org/10.1016/bs.agron.2018.02.004.

Cossani, C.M., Slafer, G.A., Savin, R., 2012. Nitrogen and water use efficiencies of wheat and barley under a Mediterranean environment in Catalonia. Field Crops Res. 128, 109–118. https://doi.org/10.1016/j.fcr.2012.01.001.
Cross, M.D., Scambos, T.A., Pacifici, F., Marshall, W.E., 2018. Validating the use of metre-scale multi-spectral satellite image data for identifying tropical forest tree species. Int. J. Remote Sens. 39, 3723–3752. https://doi.org/10.1080/01431161.2018.1448482.
Diacono, M., Rubino, P., Montemurro, F., 2013. Precision nitrogen management of wheat. A review. Agron. Sustain. Dev. 33, 219–241. https://doi.org/10.1007/s13593-012-0111-z.
El-Shikha, D.M., Waller, P., Hunsaker, D., Clarke, T., Barnes, E., 2007. Ground-based remote sensing for assessing water and nitrogen status of broccoli. Agric. Water Manag. 92, 183–193. https://doi.org/10.1016/j.agwat.2007.05.020.
FAOStat, 2020. Statistics Data: the Food and Agriculture Organization of the United Nations. Official Website. Retrieved from http://www.fao.org/faostat/en/"\|"data/QC. Accessed 3th August 2020.
Fitzgerald, G., Rodriguez, D., O'Leary, G., 2010. Measuring and predicting canopy nitrogen nutrition in wheat using a spectral index-The canopy chlorophyll content index (CCCI). Field Crops Res. 116, 318–324. https://doi.org/10.1016/j.fcr.2010.01.010.
Fois, S., Motzo, R., Giunta, F., 2009. The effect of nitrogenous fertiliser application on leaf traits in durum wheat in relation to grain yield and development. F. Crop. Res. 110, 69–75. https://doi.org/10.1016/j.fcr.2008.07.004.
Gabriel, J.L., Zarco-Tejada, P.J., López-Herrera, P.J., Pérez-Martín, E., Alonso-Ayuso, M., Quemada, M., 2017. Airborne and ground level sensors for monitoring nitrogen status in a maize crop. Biosyst. Eng. 160, 124–133. https://doi.org/10.1016/j.biosystemseng.2017.06.003.
Gamon, J.A., Penuelas, J., Field, C.B., 1992. A narrow-waveband spectral index that tracks diurnal changes in photosynthetic efficiency. Remote Sens. Environ. 41, 35–44. https://doi.org/10.1016/0034-4257(92)90059-S.
Gao, B.-C., 1996. NDWI a normalized difference water index for remote sensing of vegetation liquid water from space. Remote Sens. Environ. 7212, 257–266.
Gao, B.C., Montes, M.J., Davis, C.O., Goetz, A.F.H., 2009. Atmospheric correction algorithms for hyperspectral remote sensing data of land and ocean. Remote Sens. Environ. 113, S17–S24. https://doi.org/10.1016/j.rse.2007.12.015.
Gao, Y., Walker, J.P., Allahmoradi, M., Monerris, A., Ryu, D., Jackson, T.J., 2015. Optical sensing of vegetation water content: a synthesis study. IEEE J. Sel. Top. Appl. Earth Obs. Remote Sens. 8, 1456–1464. https://doi.org/10.1109/JSTARS.2015.2398034.
Gitelson, A.A., Kaufman, Y.J., Merzlyak, M.N., 1996. Use of a green channel in remote sensing of global vegetation from EOS-MODIS. Remote Sens. Environ. 58 (3), 289–298.
Gonzalez-Dugo, V., Durand, J.L., Gastal, F., 2009. Water deficit and nitrogen nutrition of crops. Sustain. Agric. 2, 557–575. https://doi.org/10.1007/978-94-007-0394-0_25.
Grant, O.M., Tronina, Ł., Jones, H.G., Chaves, M.M., 2007. Exploring thermal imaging variables for the detection of stress responses in grapevine under different irrigation regimes. J. Exp. Bot. 58, 815–825. https://doi.org/10.1093/jxb/erl153.
Greenwood, D.J., Lemaire, G., Gosse, G., Cruz, P., Draycott, A., Neeteson, J.J., 1990. Decline in percentage N of C3 and C4 crops with increasing plant mass. Ann. Bot. 66, 425–436. https://doi.org/10.1093/oxfordjournals.aob.a088044.
Griffin, M.K., Burke, H.K., 2003. Compensation of hyperspectral data for atmospheric effects. Lincoln Lab. J. 14, 29–54.
Gueymard, C., 1995. SMARTS, A Simple Model of the Atmospheric Radiative Transfer of Sunshine: Algorithms and Performance Assessment. Professional Paper FSEC-PF-270-95. Florida Solar Energy Center, 1679 Clearlake Road, Cocoa, FL 32922.
Gueymard, C., 2001. Parameterized transmittance model for direct beam and circumsolar spectral irradiance. Solar Energy 71 (5), 325–346.
Haboudane, D., Miller, J.R., Tremblay, N., Zarco-Tejada, P.J., Dextraze, L., 2002. Integrated narrow-band vegetation indices for prediction of crop chlorophyll content for application to precision agriculture. Remote Sens. Environ. 81, 416–426. https://doi.org/10.1016/S0034-4257(02)00018-4.
Hatfield, J.L., Gitelson, A.A., Schepers, J.S., Walthall, C.L., 2008. Application of spectral remote sensing for agronomic decisions. Agron. J. 100, 117–131. https://doi.org/10.2134/agronj2006.0370c.
Heitholt, J.J., Johnson, R.C., Ferris, D.M., 1991. Stomatal limitation to carbon dioxide assimilation in nitrogen and drought-stressed wheat. Crop Sci. 31, 135–139. https://doi.org/10.2135/cropsci1991.0011183x003100010032x.
Hoogmoed, M., Sadras, V.O., 2018. Water stress scatters nitrogen dilution curves in wheat. Front. Plant Sci. 9, 1–11. https://doi.org/10.3389/fpls.2018.00406.
Huete, A.R., 1988. A soil-adjusted vegetation index (SAVI). Remote Sens. Environ. 25, 295–309. https://doi.org/10.1016/0034-4257(88)90106-X.
Huete, A., Didan, K., Miura, T., Rodriguez, E.P., Gao, X., Ferreira, L.G., 2002. Overview of the radiometric and biophysical performance of the MODIS vegetation indices. Remote Sens. Environ. 83, 195–213. https://doi.org/10.1016/S0034-4257(02)00096-2.
Idso, S.B., 1982. Non-water-stressed baselines: a key to measuring and interpreting plant water stress. Agric. For. Meteorol. 27, 59–70. https://doi.org/10.1016/0002-1571(82)90020-6.
Idso, S.B., Jackson, R.D., Reginato, R.J., 1977. Remote-sensing of crop yields. Science 196, 19–25. https://doi.org/10.1126/science.196.4285.19.
Idso, S.B., Jackson, R.D., Pinter Jr, P.J., Reginato, R.J., Hatfield, J.L., 1981. Normalizing the stress-degree-day parameter for environmental variability. Agric. For. Meteorol. 24, 45–55. https://doi.org/10.1016/0002-1571(81)90032-7.
Jackson, R.D., Idso, S.B., Reginato, R.J., Pinter Jr, P., 1981. Canopy temperature as a crop water stress indicator. Water Resour. Res. 17, 1133–1138. https://doi.org/10.1029/WR017i004p01133.
Jackson, T.J., Chen, D., Cosh, M., Li, F., Anderson, M., Walthall, C., Doriaswamy, P., Hunt, E.R., 2004. Vegetation water content mapping using Landsat data derived normalized difference water index for corn and soybeans. Remote Sens. Environ. 92, 475–482. https://doi.org/10.1016/j.rse.2003.10.021.
Jones, H.G., 1999. Use of thermography for quantitative studies of spatial and temporal variation of stomatal conductance over leaf surfaces. Plant Cell Environ. 22, 1043–1055. https://doi.org/10.1046/j.1365-3040.1999.00468.x.
Justes, E., Mary, B., Meynard, J.M., Machet, J.M., Thelier-Huché, L., 1994. Determination of a critical nitrogen dilution curve for winter wheat crops. Ann. Bot. 74, 397–407. https://doi.org/10.1006/anbo.1994.1133.
Keeney, D.R., Nelson, D.W., 1982. Nitrogen—inorganic forms 1. Methods soil anal. Part 2. Chem. Microbiol. Prop. 5, 643–698.
Kusnierek, K., Korsaeth, A., 2015. Simultaneous identification of spring wheat nitrogen and water status using visible and near infrared spectra and Powered Partial Least Squares Regression. Comput. Electron. Agric. 117, 200–213. https://doi.org/10.1016/j.compag.2015.08.001.
Lebourgeois, V., Dupuy, S., Vintrou, É., Ameline, M., Butler, S., Bégué, A., 2017. A combined random forest and OBIA classification scheme for mapping smallholder agriculture at different nomenclature levels using multisource data (simulated Sentinel-2 time series, VHRS and DEM). Remote Sens. 9 (3), 259. https://doi.org/10.3390/rs9030259.
Lemaire, G., Jeuffroy, M.H., Gastal, F., 2008. Diagnosis tool for plant and crop N status in vegetative stage. Theory and practices for crop N management. Eur. J. Agron. 28, 614–624. https://doi.org/10.1016/j.eja.2008.01.005.
Masseroni, D., Ortuani, B., Corti, M., Gallina, P.M., Cocetta, G., Ferrante, A., Facchi, A., 2017. Assessing the reliability of thermal and optical imaging techniques for detecting crop water status under different nitrogen levels. Sustain 9, 1–20. https://doi.org/10.3390/su9091548.
Min, M., Lee, W.S., 2005. Determination of significant wavelengths and prediction of nitrogen content for citrus. Trans. Am. Soc. Agric. Eng. 48, 455–461. https://doi.org/10.13031/2013.18308.
Mistele, B., Schmidhalter, U., 2008. Estimating the nitrogen nutrition index using spectral canopy reflectance measurements. Eur. J. Agron. 29, 184–190. https://doi.org/10.1016/j.eja.2008.05.007.
Möller, M., Alchanatis, V., Cohen, Y., Meron, M., Tsipris, J., Naor, A., Ostrovsky, V., Sprintsin, M., Cohen, S., 2007. Use of thermal and visible imagery for estimating crop water status of irrigated grapevine. J. Exp. Bot. 58, 827–838. https://doi.org/10.1093/jxb/erl115.
Mon, J., Bronson, K.F., Hunsaker, D.J., Thorp, K.R., White, J.W., French, A.N., 2016. Interactive effects of nitrogen fertilization and irrigation on grain yield, canopy temperature, and nitrogen use efficiency in overhead sprinkler-irrigated durum wheat. Field Crops Res. 191, 54–65. https://doi.org/10.1016/j.fcr.2016.02.011.
Moran, M.S., Clarke, T.R., Inoue, Y., Vidal, A., 1994. Estimating crop water deficit using the relation between surface-air temperature and spectral vegetation index. Remote Sens. Environ. 49, 246–263. https://doi.org/10.1016/0034-4257(94)90020-5.
Mutanga, O., Adam, E., Cho, M.A., 2012. High density biomass estimation for wetland vegetation using WorldView-2 imagery and random forest regression algorithm. Int. J. Appl. Earth Obs. Geoinf. 18, 399–406. https://doi.org/10.1016/j.jag.2012.03.012.
Neuhaus, A., Hoogmoed, M., Sadras, V., 2017. Closing the yield gap for wheat and canola through an adjusted nitrogen nutrition index. Better Crop. With Plant Food 101, 16–18.
O'Shaughnessy, S.A., Evett, S.R., Colaizzi, P.D., 2015. Dynamic prescription maps for site-specific variable rate irrigation of cotton. Agric. Water Manag. 159, 123–138. https://doi.org/10.1016/j.agwat.2015.06.001.
Osborne, S.L., Schepers, J.S., Francis, D.D., Schlemmer, M.R., 2002. Detection of phosphorus and nitrogen deficiencies in corn using spectral radiance measurements. Agron. J. 94, 1215–1221. https://doi.org/10.2134/agronj2002.1215.
Ottman, M.J., Doerge, T.A., Martin, E.C., 2000. Durum grain quality as affected by nitrogen fertilization near anthesis and irrigation during grain fill. Agron. J. 92, 1035–1041. https://doi.org/10.2134/agronj2000.9251035x.
Quemada, M., Daughtry, C.S.T., 2016. Spectral indices to improve crop residue cover estimation under varying moisture conditions. Remote Sens. 8, 660–680. https://doi.org/10.3390/rs8080660.
Quemada, M., Gabriel, J.L., 2016. Approaches for increasing nitrogen and water use efficiency simultaneously. Glob. Food Sec. 9, 29–35. https://doi.org/10.1016/j.gfs.2016.05.004.
Quemada, M., Gabriel, J.L., Zarco-Tejada, P., 2014. Airborne hyperspectral images and ground-level optical sensors as assessment tools for maize nitrogen fertilization. Remote Sens. 6, 2940–2962. https://doi.org/10.3390/rs6042940.
R Core Team, 2021. R: A Language and Environment for Statistical Computing; R Foundation for Statistical Computing. Vienna, Austria. http://www.r-project.org/.
Raun, W.R., Solie, J.B., Stone, M.L., Martin, K.L., Freeman, K.W., Mullen, R.W., Zhang, H., Schepers, J.S., Johnson, G.V., 2005. Optical sensor-based algorithm for crop nitrogen fertilization. Commun. Soil Sci. Plant Anal. 36, 2759–2781. https://doi.org/10.1080/00103620500303988.
Ravier, C., Quemada, M., Jeuffroy, M.H., 2017. Use of a chlorophyll meter to assess nitrogen nutrition index during the growth cycle in winter wheat. Field Crops Res. 214, 73–82. https://doi.org/10.1016/j.fcr.2017.08.023.
Raya-Sereno, M.D., Ortiz-Monasterio, J.I., Alonso-Ayuso, M., Rodrigues, F.A.Jr., Rodríguez, A.A., González-Perez, L., Quemada, M., 2021. High-resolution airborne hyperspectral imagery for assessing yield, biomass, grain N concentration, and N output in spring wheat. Remote Sens. 13, 1373. https://doi.org/10.3390/rs13071373.
Rodriguez, D., Sadras, V.O., Christensen, L.K., Belford, R., 2005. Spatial assessment of the physiological status of wheat crops as affected by water and nitrogen supply using

infrared thermal imagery. Aust. J. Agric. Res. 56, 983–993. https://doi.org/10.1071/AR05035.
Rondeaux, G., Steven, M., Baret, F., 1996. Optimization of soil-adjusted vegetation indices. Remote Sens. Environ. 55, 95–107. https://doi.org/10.1016/0034-4257(95)00186-7.
Rouse Jr, J.W., Haas, R.H., Schell, J.A., Deering, D.W., 1973. Monitoring the Vernal Advancement and Retrogradation (green Wave Effect) of Natural Vegetation. NASA/GSFC, Final Report, Greenbelt, MD, USA, pp. 1–137.
Sadras, V.O., 2004. Yield and water-use efficiency of water- and nitrogen-stressed wheat crops increase with degree of co-limitation. Eur. J. Agron. 21, 455–464. https://doi.org/10.1016/j.eja.2004.07.007.
Sadras, V.O., Lemaire, G., 2014. Quantifying crop nitrogen status for comparisons of agronomic practices and genotypes. F. Crop. Res. 164, 54–64. https://doi.org/10.1016/j.fcr.2014.05.006.
Sanad, M.N.M.E., Smertenko, A., Garland-Campbell, K.A., 2019. Differential dynamic changes of reduced trait model for analyzing the plastic response to drought phases: a case study in spring wheat. Front. Plant Sci. 10, 1–19. https://doi.org/10.3389/fpls.2019.00504.
Schepers, J.S., Blackmer, T.M., Wilhelm, W.W., Resende, M., 1996. Transmittance and reflectance measurements of corn leaves from plants with different nitrogen and water supply. J. Plant Physiol. 148, 523–529. https://doi.org/10.1016/S0176-1617(96)80071-X.
Seligman, N.G., Loomis, R.S., Burke, J., Abshahi, A., 1983. Nitrogen nutrition and canopy temperature in field-grown spring wheat. J. Agric. Sci. 101, 691–697. https://doi.org/10.1017/S0021859600038727.
Sims, D.A., Gamon, J.A., 2002. Relationships between leaf pigment content and spectral reflectance across a wide range of species, leaf structures and developmental stages. Remote Sens. Environ. 81, 337–354. https://doi.org/10.1016/S0034-4257(02)00010-X.
Sticksel, E., Maidl, F.X., Retzer, F., Fischbeck, G., 1999. Nitrogen uptake and utilization in winter wheat under different fertilization regimes, with particular reference to main stems and tillers. J. Agron. Crop Sci. 183, 47–52. https://doi.org/10.1046/j.1439-037X.1999.00320.x.
Constable, G., Rawson, H., 1980. Effect of leaf position, expansion and age on photosynthesis, transpiration and water use efficiency of cotton. Funct. Plant Biol. 7, 89–100. https://doi.org/10.1071/pp9800089.
Tanner, C.B., 1963. Plant temperatures 1. Agron. J. 55, 210–211. https://doi.org/10.2134/agronj1963.00021962005500020043x.
Tanner, C.B., Sinclair, T.R., 1983. Efficient Water use in crop production: research or Re-search? In: Taylor, H.M., Jordan, W.R., Sinclair, T.R. (Eds.), Limitations to Efficient Water Use in Crop Production. Am. Soc. Agron, pp. 1–27. https://doi.org/10.2134/1983.limitationstoefficientwateruse.c1.
Tilling, A.K., O'Leary, G.J., Ferwerda, J.G., Jones, S.D., Fitzgerald, G.J., Rodriguez, D., Belford, R., 2007. Remote sensing of nitrogen and water stress in wheat. Field Crops Res. 104, 77–85. https://doi.org/10.1016/j.fcr.2007.03.023.
Walker, G.K., 1980. Relation between Crop Temperature and the Growth and Yield of Kidney Beans (Phaseolus Vulgaris L.) Ph.D Thesis. University of California, Davis, CA, 203 pp.
Weiss, M., Jacob, F., Duveiller, G., 2020. Remote sensing for agricultural applications: a meta-review. Remote Sens. Environ. 236, 111402. https://doi.org/10.1016/j.rse.2019.111402.
World Reference Base for Soil Resources, 2014. International Soil Classification Systems for Naming Soils and Creating Legends for Soil Maps, World Soil Resources Reports No. 106. FAO, Rome.
Zadoks, J.C., Chang, T.T., Konzak, C.F., 1974. A decimal code for the growth stage of cereals. Weed Res. 14, 415–421. https://doi.org/10.1111/J.1365-3180.1974.TB01084.X.
Zarco-Tejada, P.J., Miller, J.R., Noland, T.L., Mohammed, G.H., Sampson, P.H., 2001. Scaling-up and model inversion methods with narrowband optical indices for chlorophyll content estimation in closed forest canopies with hyperspectral data. IEEE Trans. Geosci. Remote Sens. 39, 1491–1507. https://doi.org/10.1109/36.934080.
Zarco-Tejada, P.J., Hornero, A., Hernández-Clemente, R., Beck, P.S.A., 2018. Understanding the temporal dimension of the red-edge spectral region for forest decline detection using high-resolution hyperspectral and Sentinel-2a imagery. ISPRS J. Photogramm. 137, 134–148. https://doi.org/10.1016/j.isprsjprs.2018.01.017.
Zhao, C., Liu, L., Wang, J., Huang, W., Song, X., Li, C., 2005. Predicting grain protein content of winter wheat using remote sensing data based on nitrogen status and water stress. Int. J. Appl. Earth Obs. Geoinf. 7, 1–9. https://doi.org/10.1016/j.jag.2004.10.002.
Ziadi, N., Bélanger, G., Claessens, A., Lefebvre, L., Cambouris, A.N., Tremblay, N., Nolin, M.C., Parent, L.É., 2010. Determination of a critical nitrogen dilution curve for spring wheat. Agron. J. 102, 241–250. https://doi.org/10.2134/agronj2009.0266.
Zillmann, E., Graeff, S., Link, J., Batchelor, W.D., Claupein, W., 2006. Assessment of cereal nitrogen requirements derived by optical on-the-go sensors on heterogeneous soils. Agron. J. 98, 682–690. https://doi.org/10.2134/agronj2005.